CONF-891204--8
PNL-SA-17021

DISCLAIMER

MICROSTRUCTURAL EXPLANATION FOR IRRADIATION EMBRITTLEMENT OF V-15Cr-5Ti

PNL-SA--17021

DE90 004112

D.S. Gelles
S. Ohnuki (a)
B.A. Loomis (b)
H. Takahashi (a)
F.A. Garner

November 1989

International Conference for
Fusion Reactor Materials
Kyoto, Japan
December 4-8, 1989

Work supported by the U.S. Department of Energy
under Contract DE-AC06-76RLO 1830

Pacific Northwest Laboratory
Richland, Washington 99352

(a) Hokkaido University, Japan
(b) Argonne National Laboratory

A MICROSTRUCTURAL EXPLANATION FOR IRRADIATION EMBRITTLEMENT OF V-15Cr-5Ti

D. S. Gelles,* S. Ohnuki,** B. A. Loomis,*** H. Takahashi,**
and F. A. Garner*

* Materials Science Department, Pacific Northwest Laboratory(a),
P.O. Box 999, Richland, WA 99352, USA
** Metals Research Institute, Faculty of Engineering,
Hokkaido University, Sapporo 060, Japan
*** Fusion Power Program, Argonne National Laboratory,
Argonne, IL 60439, USA

Abstract

Vanadium alloys are candidate materials for first wall fusion reactor applications based on low induced activity and heat resistant response. However, recent results have indicated that modest levels of neutron irradiation damage in V-15Cr-5Ti lead to severe degradation of mechanical properties. In order to explain the observed behavior, specimens of V-15Cr-5Ti have been examined by transmission electron microscopy following irradiation at 600°C to 14 dpa in the Fast Flux Test Facility (FFTF). The conditions examined included two heats of V-15Cr-5Ti with very different oxygen contents and, in one case, a section of a charpy specimen demonstrated to have very poor impact resistance. Specimens irradiated at 420 and 520°C were also examined to confirm density change measurements that indicated swelling levels as high as 2.5%.

Following irradiation at 600°C, a complex microstructure was found that included a perfect dislocation network of line segments and loops, faulted loops, a high density of black spot damage and a high density of rod-shaped precipitates. Heat-to-heat variations did not appear to significantly alter these microstructural features; instead the density of large blocky precipitates, believed to be TiO_2, was found to have increased with increasing oxygen content. Only two of the specimens irradiated at 600°C contained voids, whereas none of the specimens irradiated at 420 or 520°C contained voids. Therefore, swelling as measured by density change is probably due to phase instability in these specimen conditions, and the hardening and irradiation embrittlement that has been observed can be explained by the microstructural development. Phase stability appears to be an important criterion in the design of vanadium alloys for fusion applications.

(a) Operated for the U.S. Department of Energy by Battelle Memorial Institute under Contract DE-AC06-76RLO 1830.

A MICROSTRUCTURAL EXPLANATION FOR IRRADIATION EMBRITTLEMENT OF V-15Cr-5Ti -

D. S. Gelles (Pacific Northwest Laboratory),[1] S. Ohnuki (Hokkaido University, Japan), B. A. Loomis (Argonne National Laboratory), H. Takahashi (Hokkaido University, Japan) and F. A. Garner (Pacific Northwest Laboratory)

OBJECTIVE

The objective of this effort is to determine the suitability of low activation vanadium alloys for first wall applications.

SUMMARY

Recent results have indicated that modest levels of neutron irradiation damage in V-15Cr-5Ti lead to severe degradation of mechanical properties. In order to explain the observed behavior, specimens of V-15Cr-5Ti have been examined by transmission electron microscopy following irradiation at 600°C to 14 dpa in the Fast Flux Test Facility (FFTF). The conditions examined included two heats of V-15Cr-5Ti with very different oxygen contents and, in one case, a section of a charpy specimen demonstrated to have very poor impact resistance. Specimens irradiated at 420 and 520°C were also examined to confirm density change measurements that indicated swelling levels as high as 2.5%.

Following irradiation at 600°C, a complex microstructure was found that included a perfect dislocation network of line segments and loops, faulted loops, a high density of black spot damage and a high density of rod-shaped precipitates. Heat-to-heat variations did not appear to significantly alter these microstructural features; instead the density of large blocky precipitates, believed to be TiO_2, was found to have increased with increasing oxygen content. Only two of the specimens irradiated at 600°C contained voids, whereas none of the specimens irradiated at 420 or 520°C contained significant void swelling. Therefore, swelling as measured by density change is probably due to phase instability in these specimen conditions, and the hardening and irradiation embrittlement that have been observed can be explained by the microstructural development. Phase stability appears to be an important criterion in the design of vanadium alloys for fusion applications.

PROGRESS AND STATUS

Introduction

Vanadium alloys are candidate materials for first wall fusion reactor applications[1] based on low induced activity[2] and heat resistant response.[3] However, recent results have indicated that neutron irradiation damage in vanadium alloys leads to degradation of mechanical properties.[4-8] The most severe degradation was found in the most promising alloy, V-15Cr-5Ti. It is

---

1 Operated for the U.S. Department of Energy by Battelle Memorial Institute under Contract DE-AC06-76RLO 1830.

not yet understood what has caused this mechanical property degradation. Two possibilities have been suggested: oxygen contamination and hydrogen embrittlement.[9,10] However, an earlier paper had shown that hydrogen contamination was less severe in V-15Cr-5Ti than in other vanadium alloys because the hydrogen did not diffuse into the alloy as extensively; therefore, the greater loss of ductility exhibited by the V-15Cr-5Ti after neutron irradiation, in comparison to the V-3Ti-0.5Si and V-20Ti alloys, is not attributable to an increased H concentration.[11]

It was the original intent of the present effort to examine irradiated V-15Cr-5Ti microstructures in order to assess the consequences of solute segregation and dislocation evolution on embrittlement. This work was done concurrently with microstructural examinations of simpler vanadium alloys irradiated under the same conditions,[12] so that comparisons with less embrittled microstructures can be made. The available specimen matrix included two heats of V-15Cr-5Ti with different oxygen levels, and different specimens of the same material irradiated in different capsules so as to give somewhat different dose levels and hydrogen absorption levels. Compositions for the alloys that were examined are given in Table 1. It was also possible to examine the microstructure of an embrittled charpy specimen to eliminate the possibility that the Charpy specimens were mishandled during manufacture.

Recently, density change measurements were reported for a series of V-15Cr-5Ti specimens irradiated at 420, 520 or 600°C to about 15 dpa.[13] The results, reproduced in Table 2, indicated levels of swelling as high as 2.4%. As a result, the present effort was expanded to include microstructural examination of several of the specimens of interest, in order to explain the large variation in swelling that was found.

Experimental Procedures

Compositions of the specimens selected for examination are listed in Table 1. These specimens were irradiated in the form of either standard transmission electron microscopy (TEM) disks or miniature charpy specimens which were immersed in lithium and contained in molybdenum alloy capsules. The capsules were identified as V420, V519, V521, V624 and V627, and all TEM specimens in a given capsule were engraved with the same location code: LR, LV, LX, LZ and L1, respectively. Irradiation was performed in the FFTF/MOTA during cycles 7 and 8. Capsule V420 was in level 2, canister C, basket 4 designed to operate at 420°C, but actually at 406°C. Capsules V519 and V521 were in level 1, canister B, basket 1 and basket 3, respectively, both designed to operate at 520°C. The actual operating temperature was 520°C. Capsules V624 and V627 were in level 5, canister D, basket 3 and basket 2, respectively, designed to operate at 600°C. The actual operating temperature was 601°C. However, during irradiation in the middle of cycle 7, specimens underwent a temperature excursion to 676°C in level 1, canister B and to 798-806°C in level 5, canister D, for 50 minutes. Therefore, specimens irradiated at 520°C were briefly heated 156° and specimens irradiated at 600°C were briefly heated 206°C. The accumulated neutron fluences were 5.19, 4.33, 3.57, 2.96 and 2.39 x 10^{22} n/cm^2 ($E > 0.1$ MeV), respectively, corresponding to doses of 30.6, 25.6, 21.1, 17.4 and 14.1 dpa. Following irradiation, specimens were removed and cleaned. One specimen of each alloy was assigned for density

change measurement and the second was provided for TEM. Specimen conditions selected for examination, irradiation history and results of density measurement are listed in Table 2.

Specimen preparation followed standard electropolishing procedures using a twin jet polishing unit with a solution of 20% sulfuric acid in methanol. Microstructural examinations were performed on a 200 KeV transmission electron microscope, and compositional analyses employed a scanning transmission electron microscope operating at 120 KeV, fitted with a standard x-ray detector coupled to an analyzing computer. Beam positions for compositional scans were controlled manually.

Results

Void Swelling

The density change measurements given in Table 2 indicate variations in density of up to 2% for nominally similar specimens irradiated under similar conditions. The maximum measured was 2.39% for heat ANL114 at 520°C and 21 dpa, but the same heat reached 1.56% at 420°C and 31 dpa; heat CAM834 had 1.4% at 420°C and 31 dpa. All other measurements were on the order of 0.5% or less. Comparison of these results with alloy composition information in Table 1 suggests that the alloy with the lowest impurity level gave the largest decrease in density, in agreement with conclusions drawn for simpler alloys.[12]

However, transmission electron microscopy observations were unable to confirm density changes in excess of 1% were due to cavity formation, or that cavity formation was even a prominent microstructural development in V-15Cr-5Ti. Of the specimens listed in Table 2, all conditions except XHLR, XFLX and XLL1 were successfully prepared for transmission electron microscopy. Only specimen XHL1 of heat ANL114, irradiated at 600°C to 14 dpa, had developed a well defined uniform array of voids. The remaining specimens either contained only a few voids, non-uniformly distributed, or none at all. In cases where only a few voids were found, they were generally associated with blocky precipitate similar to the situation seen in simpler alloys.[12]

Examples of microstructures found in specimens XKLR, XHLX and XHL1 are given in Figure 1. Figures 1a and 1b show specimen XKLR, of heat CAM834 irradiated at 420°C to 30.6 dpa. This specimen condition had 1.4% density change. The microstructure is shown in void contrast in Figure 1a. A few small voids marked by arrows and a number of surface pits can be identified. Figure 1b shows another area in dislocation contrast. The dislocation structure is complex, including dislocation loops, tangles, and black spot damage. Figures 1c and 1d provide similar information for specimen XHLX (heat ANL114 irradiated at 520°C and 21 dpa) that had 2.39% swelling as measured by density change. In Figure 1c, several large cavities can be seen associated with a large spherical precipitate. However, the rest of the microstructure contains negligible cavitation, and an explanation for the density change results is not apparent. The dislocation structure, shown in Figure 1d, contains dislocation loops, tangles, and black spot damage, but the structure is coarser than that formed at 420°C. Figure 1e provides an example of the structure in the same alloy following irradiation at 600°C and 14 dpa where 0.33% density change was observed. A moderate density of small cavities as

large as 4 nm can be seen. Therefore, it must be presumed that the density change measurements that implied void swelling levels as high as 2.4% were not really due to void swelling.

Microstructural evolution at 600°C

Due to the complexity of the microstructure, the major emphasis of microstructural examinations was shifted to the highest available irradiation temperature of 600°C, in order to provide the least complicated microstructure with the largest features for examination. Several conditions were examined in order to evaluate the tendency for heat-to-heat and specimen-to-specimen variations. The specimens were XKLZ and XKLI of heat CAM834, irradiated in different capsules; specimen XLLZ of heat ANL101, irradiated adjacent to specimen XKLZ; specimen XFL1 of heat CAM835, used for compositional analysis; and a section from charpy specimen RH35 of heat CAM835, which had been tested at 240°C and gave brittle response indicating a ductile brittle transition temperature (DBTT) above 240°C.

Figure 2 provides a series of micrographs for an area near an (011) orientation in specimen XKLZ of heat CAM834 with moderate impurity content, irradiated at 600°C to 17.4 dpa. Figure 2a shows the microstructure in $\bar{g}$ = 01$\bar{1}$ dislocation contrast. The structure contains a complex dislocation tangle and black spot damage. The same area is shown in dark field $\bar{g}$ = 01$\bar{1}$ contrast (approaching weak beam) in Figure 2b, and in dark field $\bar{g}$ = 200 contrast in Figure 2c. Comparison of Figures 2b and 2c demonstrates that a complex dislocation structure is present, containing stacking fault features on at least two different planes (visible only in <011> contrast), and a complex dislocation tangle. Stereo analysis of the planar defects indicates that these faults are probably on {110} planes. Stacking fault features in vanadium alloys are expected to indicate the presence of precipitate particles that were formed during irradiation.

Figure 3 shows a second area near an (001) orientation in specimen XKLZ. Figure 3a provides an image in $\bar{g}$ = 110 dislocation contrast that is remarkable for the short straight features that can be seen along with the dislocation tangles and black spot damage. The straight features lie in <100> directions. They appear apparently as a result of <100> rel rods found in the diffraction pattern and therefore are a result of either planar defects on {100} planes or needles in <100> directions. Dark field images of the features forming the rel rod spots are shown in Figures 3b and 3c for two orthogonal orientations. The images are as long as 40 nm, often consisting of a series of small spots, indicative of precipitate interactions. Therefore, evidence both for precipitation on {110} planes and either on {100} planes or in <110> directions is indicated. Figures 3d and 3e provide the corresponding $\bar{g}$ = 110 and 200 dark field dislocation contrast images, showing dislocation tangles similar to those in Figures 2b and 2c. However, faulted images do not appear in either micrograph. The reason why the faulted images in $\bar{g}$ = 110 contrast appear for 011 foil orientations and not for 001 foil orientations is not yet understood.

The dislocation and rel rod images were examined to a lesser extent in specimens XKL1, XLLZ, XFL1 and RH35 and were found to be similar in appearance and scale. In order to demonstrate the similarities, Figures 4, 5 and 6 have been prepared to show similar rel rod images in specimens XKL1,

XLLZ, and RH35, respectively. Figure 4 provides a bright field image in 4a and two dark field images in 4b and 4c using dark field contrast from orthogonal rel rods for a thicker foil near an (001) orientation. The specimen identity is XKL1, corresponding to the same heat as that shown in Figures 2 and 3, but following irradiation in a different capsule to a somewhat higher dose. The rel rod images in Figures 3 and 4 are similar in size and distribution. Therefore, minor differences in irradiation history have little effect on precipitation response of the rel rod features found in V-15Cr-5Ti.

Figure 5 gives similar images for specimen XLLZ, made from heat ANL101 and irradiated in the same capsule as specimen XKL1. The main differences between heats ANL101 and CAM834 are in impurity content: ANL101 contains higher oxygen and carbon levels, and CAM834 contains a higher silicon level. Figures 5a and 5b show bright and dark field rel rod images and Figure 5c provides dark field contrast for the orthogonal rel rod images. The images in Figure 5 are similar to those in Figure 4 except that a second fine precipitate is distributed more uniformly in Figure 5.

The microstructure of specimen RH35 was found to be similar to that of XHL1 and different from other conditions of V-15Cr-5Ti because void swelling was found in one large area of the specimen, with some voids as large as 30 nm. RH35 was made from heat CAM835, which is similar in composition to CAM834 but not as pure as ANL114. The void swelling in RH35 is shown in Figure 6a, to be compared with that in Figure 1e at much higher magnification. However, dislocation and rel rod images were similar to other conditions of V-15Cr-5Ti irradiated at 600°C. Examples of dislocation contrast and dark field rel rod contrast for the orthogonal rel rod images are given in Figures 6b, 6c and 6d. These images are very similar in size and distribution to those from the other specimens examined.

Therefore, except for differences in void development, all of the conditions of V-15Cr-5Ti examined following irradiation at 600°C had similar microstructures, and the microstructures were sufficiently complex to provide adequate explanation for irradiation hardening and post-irradiation embrittlement, as were observed in Charpy and tensile tests.

In the course of microstructural examinations, it was found that a low density of very large precipitate particles were present in several of the specimens, distributed nonuniformly. Examples are provided in Figure 7. Specimen XLL1 of heat ANL101, which had the highest oxygen content, is shown in Figure 7a, compared with specimens XKLZ and RH35 of heats CAM834 and CAM835, which had similar lower oxygen contents, in Figures 7b and 7c, respectively. It is assumed that these particles are TiO_2, based on the observation that the highest density of particles was found in heat ANL101, which had the highest oxygen content. If the oxygen in V-15Cr-5Ti is retained as large particles after melting procedures, then oxygen levels would not be expected to have a significant consequence on mechanical properties in this alloy, except that crack nucleation at such particles may be facilitated, and the Ductile Brittle Transition Temperature (DBTT) would be increased.

Microchemical Analysis

Specimen XFL1 was analyzed to provide results on microchemical segregation in the vicinity of a grain boundary. The results are shown in Figure 8, giving titanium and chromium concentrations as a function of distance from the grain boundary (G.B.) for an area containing a grain boundary. Figure 8 demonstrates that titanium levels are higher at the grain boundary and lower adjacent to the boundary, whereas chromium concentrations are relatively unaffected, with perhaps slight enhancement adjacent to the boundary. Therefore, titanium tends to segregate towards all point defect sinks, and chromium tends not to segregate. The effective diffusion distance for segregation at 600°C to 14 dpa is on the order of 200 nm based one the extent of the denuded zone.

DISCUSSION

The purpose of this effort was to provide an explanation for the severe irradiation embrittlement observed in V-15Cr-5Ti in comparison to other vanadium alloys of interest. Several specimens of V-15Cr-5Ti comprising different heats and somewhat different irradiation conditions have been examined by electron microscopy and an explanation based on rather complex microstructural development can now be given. Microstructural observations on V-15Cr-5Ti irradiated at 600°C to about 15 dpa may be summarized as follows. Void swelling is rarely observed, and then, apparently only in purer alloys. Dislocation structures consist of climbing dislocation loops and tangles. However, in the course of imaging dislocation structures, other features are found: 1) stacking fault features, apparently on {011} planes, 2) rel rod features (either platelets on {001} planes or needles in <001> directions) which indicate precipitate formation, and 3) as black spot damage, also which also indicates precipitate formation. The density of these features is considerably higher than those found in simpler alloys,[12] and therefore, greater irradiation hardening is expected in V-15Cr-5Ti than in other vanadium alloys of interest. Irradiation hardening can explain the large DBTT shifts found in this alloy following irradiation.

It can be argued that insufficient control of hydrogen or oxygen impurity levels is responsible for the observed embrittlement. Certainly, data can be produced to demonstrate that hydrogen and oxygen intake lead to increased embrittlement. However, these arguments are not expected to apply in the present situation. Hydrogen intake has been found to be more restricted to surface layers in V-15Cr-5Ti than in V-3Ti-0.5Si,[11] for specimens which were surface-ground in contact with water at room temperature. In those experiments, hydrogen levels in V-15Cr-5Ti were found to have been reduced from 12 a/o at the surface to about 0.4 a/o at a distance of 20 μm from the surface. Since hydrogen levels in V-15Cr-5Ti are known to be reduced from exposure to lithium,[11] it can be assumed that if hydrogen is responsible for embrittlement in the mechanical property specimens, hydrogen intake must have occurred following irradiation during cleaning operations at room temperature. Any significant hydrogen absorption is therefore probably restricted to the vicinity of specimen surfaces. Hydrogen adsorption at specimen surfaces is not expected to produce the embrittlement observed following irradiation.

The excessive oxygen levels in the V-15Cr-5Ti alloys that were tested may also be responsible for such embrittlement. However, if the interpretation of the observations of large precipitate particles is correct, then oxygen tends to be tied up in large TiO_2 precipitate particles, and the bulk oxygen levels probably do not account for the unusually poor postirradiation mechanical properties found in V-15Cr-5Ti.

A microstructural explanation for excessive irradiation embrittlement of V-15Cr-5Ti specimens is suggested based on the complex microstructure observed. V-15Cr-5Ti does indeed have a more complex microstructure following irradiation at 600°C to about 15 dpa in the FFTF/MOTA compared with simpler vanadium alloys. This difference is probably a result of decreased phase stability. The large density change measurements that cannot be accounted for by void swelling are also probably a consequence of phase instability. The density of V-Cr-Ti alloys is a steep function of Cr and Ti such that segregation and/or precipitation could easily lead to large density changes. The complex microstructure alone would explain the poor postirradiation mechanical properties of V-15Cr-5Ti in comparison with simpler vanadium alloys.

It is interesting to speculate on the cause. The rel rod structure found in V-15Cr-5Ti has similarities to precipitates found in V-10Ti and V-20Ti.[12] If these features are both due to titanium precipitation, then the fault features on {011} planes may be a result of chromium precipitation. Irradiation hardening could result from the segregation of both major alloying additions to precipitates which form obstacles to deformation. If this argument is correct, the only way to solve this irradiation embrittlement problem in V-15Cr-5Ti is by improved alloy design. Other alloying options must be considered rather than chromium and titanium.

CONCLUSIONS

A complex microstructure was found in V-15Cr-5Ti specimens following irradiation at 600°C to doses of about 15 dpa. The structure included a perfect dislocation network of climbing line segments and loops, faulted loops, a high density of black spot damage and a high density of rod-shaped precipitates. Heat-to-heat variations did not appear to significantly alter these microstructural features; instead the density of large blocky precipitates, believed to be TiO_2, increased with increasing oxygen content. Two of the specimens irradiated at 600°C contained voids but the accumulated swelling was low, whereas none of the specimens irradiated at 420 or 520°C contained significant void swelling. Therefore, swelling as measured by density change is probably due to phase instability in these specimen conditions, and the hardening and irradiation embrittlement that have been observed can be explained by the microstructural development. Phase stability appears to be an important criterion in the design of vanadium alloys for fusion applications.

FUTURE WORK

This work will be continued when warranted.

References

1. R. E. Gold, D. L. Harrod, R. L. Ammon, R. W. Buckman, Jr. and R. C. Svedberg, "Technical Assessment of Vanadium-base Alloys for Fusion Reactor Applications," COO-4540-1(Vol. 1) April 1978, Westinghouse Electric Corporation, Pittsburgh, PA.

2. R. W. Conn, "First Wall and Divertor Plate Selection in Fusion Reactors," J. Nucl. Mater., 76 & 77 (1978) 103-11.

3. D. L. Harrod and R. E. Gold, "Mechanical Properties of Vanadium and Vanadium-base Alloys," International Metals Reviews, No. 4 (1980) 163-221.

4. D. N. Braski, "The Effect of Neutron Irradiation on Vanadium Alloys," J. Nucl. Mater., 141-143 (1986) 1125-31.

5. N. S. Cannon, M. L. Hamilton, A. M. Ermi, D. S. Gelles and W. L. Hu, "Influence of Neutron Irradiation on the Charpy Impact Properties of V-15Cr-5Ti," J. Nucl. Mater., 155-157 (1988) 987-91.

6. H. Matsui, O. Yoshinari and K. Abe, "Radiation Hardening of Vanadium by 14 MeV Neutrons," J. Nucl. Mater., 155-157 (1988) 855-9.

7. H. Takahashi, S. Ohnuki, H. Kinoshita, R. Nagasaki and K. Abe, "The Effects of Damage Structures on Mechanical Properties of Neutron Irradiated Vanadium," J. Nucl. Mater., 155-157 (1988) 982-6.

8. D. N. Braski, "The Effect of Neutron Irradiation on the Tensile Properties and Microstructure of Several Vanadium Alloys," Influence of Radiation on Materials Properties: 13th International Symposium (Part II), ASTM STP 956, F. A. Garner, C. H. Henager and N. Igata, Eds., American Society for Testing and Materials, Philadelphia, PA 1987, 271-90.

9. B. A. Loomis, R. H. Lee and D. L. Smith, "Strength, Ductility and Ductile-Brittle Transition Temperature for MFR Candidate Vanadium Alloys," in Fusion Reactor Materials Semiannual Progress Report of Period Ending September 30, 1987, DOE/ER-0313/3, 246-253.

10. B. A. Loomis, B. J. Kestel, B. D. Edwards and D. L. Smith, "Temperature Dependence of the Fracture Behavior and the DBTT of Dehydrogenated and Hydrogenated Vanadium-Base Alloys," in Fusion Reactor Materials Semiannual Progress Report of Period Ending September 30, 1988, DOE/ER-0313/5, 242-255.

11. B. A. Loomis, A. B. Hull, O. K. Chopra and D. L. Smith, "Hydrogen Concentration Distribution in Vanadium-Base Alloys After Surface Preparation and Exposure to Liquid Lithium," in Fusion Reactor Materials Semiannual Progress Report of Period Ending March 31,1988, DOE/ER-0313/4, 160-167.

12. S. Ohnuki, D. S. Gelles, B. A. Loomis, F. A. Garner and H. Takahashi, "Microstructural Examination of Simple Vanadium Alloys Irradiated in the FFTF/MOTA," companion paper in this report, PNL-SA-17020FP.

13. B. A. Loomis, D. L. Smith and F. A. Garner, "Swelling of Neutron-Irradiated Vanadium Alloys, in Fusion Reactor Materials Semiannual Progress Report of Period Ending March 31, 1989, DOE/ER-0313/6, 339-348.

Table 1. Alloy compositions for V-15Cr-5Ti heats.

ANL ID #	Melt Number	Base Alloy	Impurity concentration O	N	C	Si	Fe
BL-21	CAM835	V-13.7Cr-4.8Ti	340	510	180	1150	300
BL-22	ANL114	V-13.4Cr-5.1Ti	300	52	150	56	140
BL-23	CAM834	V-12.9Cr-5.9Ti	400	490	280	1230	420
BL-24	ANL101	V-13.5Cr-5.2Ti	1190	360	500	390	520

Table 2. Specimen conditions of V-15Cr-5Ti selected for microstructural examination. Swelling values based on density change measurements are included where available.

Specimen ID	ANL ID #	Heat Number	Capsule Number	Irradiation Temperature (°C)	Dose[a] (dpa)	Swelling (%)
XLLR	BL-24	ANL101	V420	420	30.6	0.0
XKLR	BL-23	CAM834	V420	420	30.6	1.4
XHLR	BL-22	ANL114	V420	420	30.6	1.56
XFLR	BL-21	CAM835	V420	420	30.6	0.44
XLLV	BL-24	ANL101	V519	520	25.6	0.36
XKLX	BL-23	CAM834	V521	520	21.1	0.55
XHLX	BL-22	ANL114	V521	520	21.1	2.39
XFLX	BL-21	CAM835	V521	520	21.1	0.63
XLL1	BL-24	ANL101	V627	600	14.1	0.0
XKL1	BL-23	CAM834	V627	600	14.1	NM
XKLZ	BL-23	CAM834	V624	600	17.4	0.28
XHL1	BL-22	ANL114	V627	600	14.1	0.33
XFL1	BL-21	CAM835	V627	600	14.1	0.42[c]
XLLZ	BL-24	ANL101	V624	600	17.4	NM
RH35[b]	BL-24	CAM835	V624	600	17.4	NM

NM = not measured.
a = based on 5.9 dpa/ 10^{22} n•cm^{-2}, (E > 0.1 MeV).
b = section from Charpy specimen.
c = density measurement for specimen XFLZ at 17.4 dpa.

FIGURE CAPTIONS

Figure 1. Examples of specimen microstructures. Specimen XKLR from heat CAM834 irradiated at 420°C is shown (a) in void contrast and (b) in 01$\bar{1}$ dislocation contrast. Specimen XHLX from heat ANL114 irradiated at 520°C is shown (c) in void contrast and (d) in 01$\bar{1}$ dislocation contrast. Specimen XHL1 also from heat ANL114 irradiated at 600°C is shown in void contrast.

Figure 2. Specimen XKLZ from heat CAM834 irradiated at 600°C to 17.4 dpa in (a) 01$\bar{1}$ bright field and (b) dark field dislocation contrast and in (c) 200 dark field contrast for a foil near (011).

Figure 3. Specimen XKLZ from heat CAM834 irradiated at 600°C to 17.4 dpa in (a) 110 bright field dislocation contrast, in (b) and (c) in <200> rel rod dark field contrast for orthogonal rel rods and (d) 200 dark field dislocation contrast in a foil near (001).

Figure 4. Specimen XKL1 from heat CAM834 irradiated at 600°C to 14.1 dpa in (a) bright field and in (b) and (c) in <200> rel rod dark field contrast for orthogonal rel rods in a foil near (011).

Figure 5. Specimen XLLZ from heat ANL101 irradiated at 600°C to 17.4 dpa in (a) bright field and in (b) and (c) in <200> rel rod dark field contrast for orthogonal rel rods in a foil near (011).

Figure 6. Charpy specimen RH35 from heat CAM835 irradiated at 600°C to 17.4 dpa in (a) void contrast, in (b) 110 bright field dislocation contrast and in (c) and (d) in <200> rel rod dark field contrast for orthogonal rel rods in a foil near (011).

Figure 7. Low magnification examples of blocky precipitates in (a) specimen XLL1 from heat ANL101, in (b) specimen XKLZ from heat CAM834 and in (c) specimen RH35 from heat CAM835.

Figure 8. Microchemical segregation in the vicinity of a grain boundary in V-15Cr-5Ti specimen XFL1 following irradiation at 600°C to 14.1 dpa.2

T-1 Q. 7

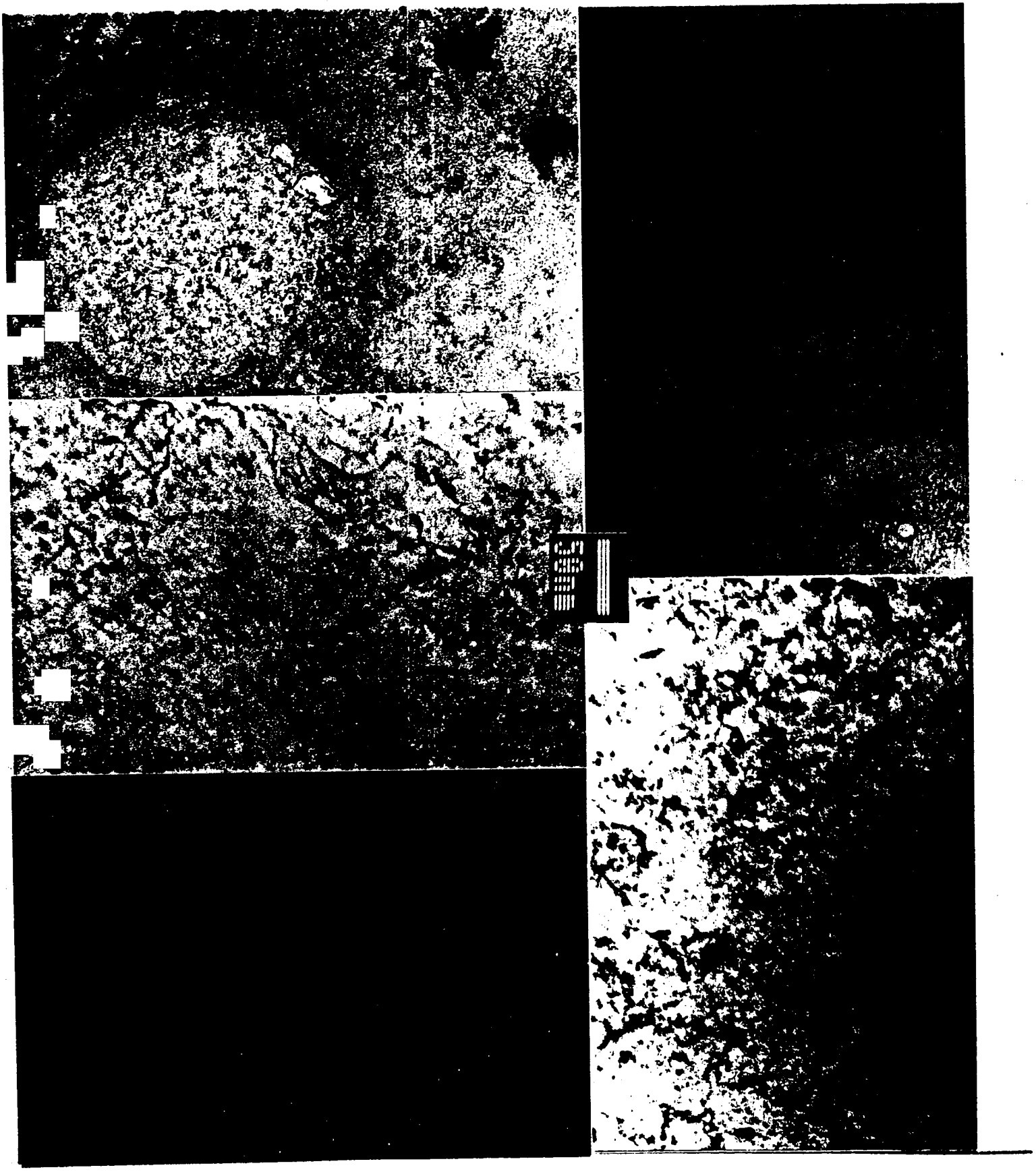

Fig 2

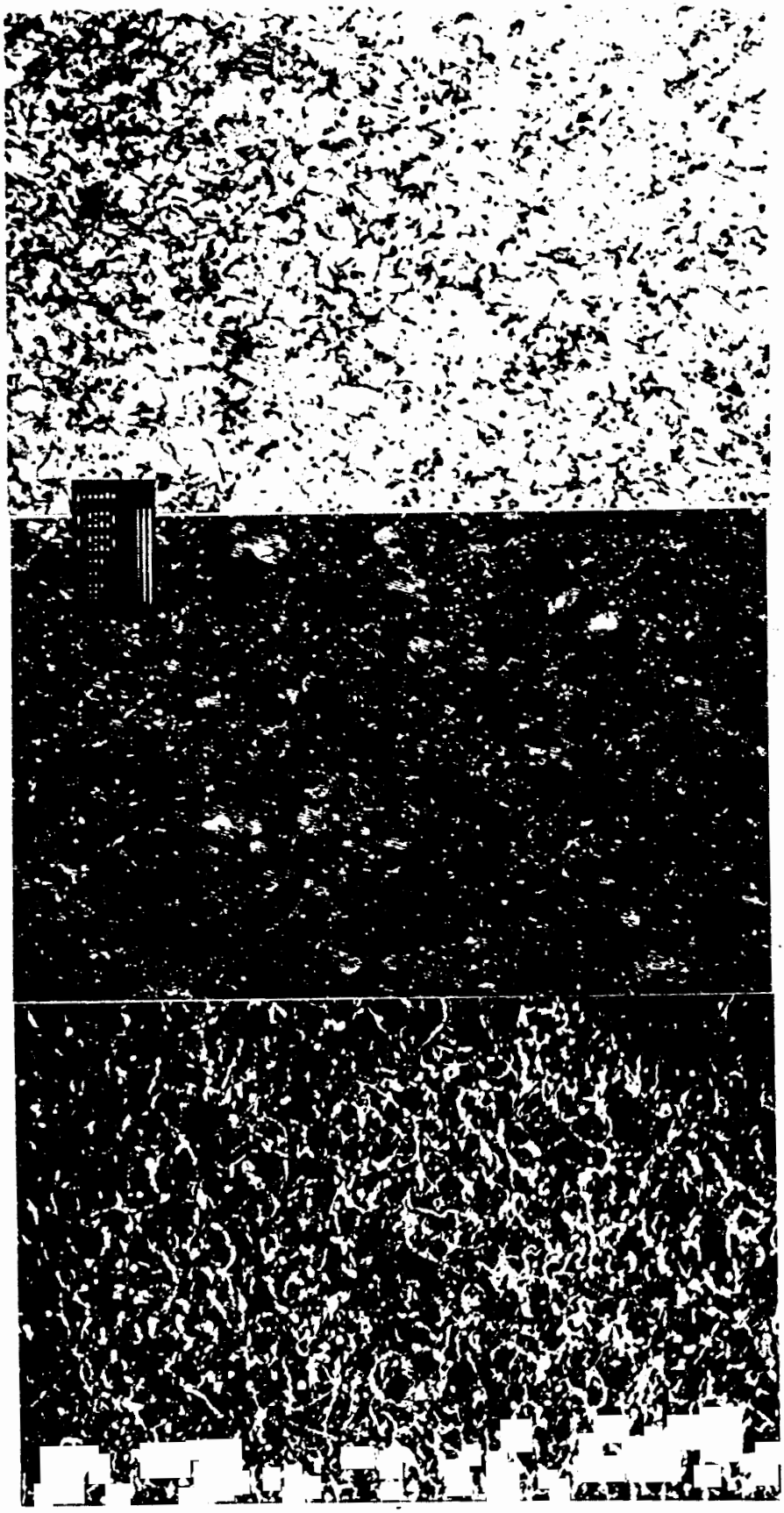

Fig 3

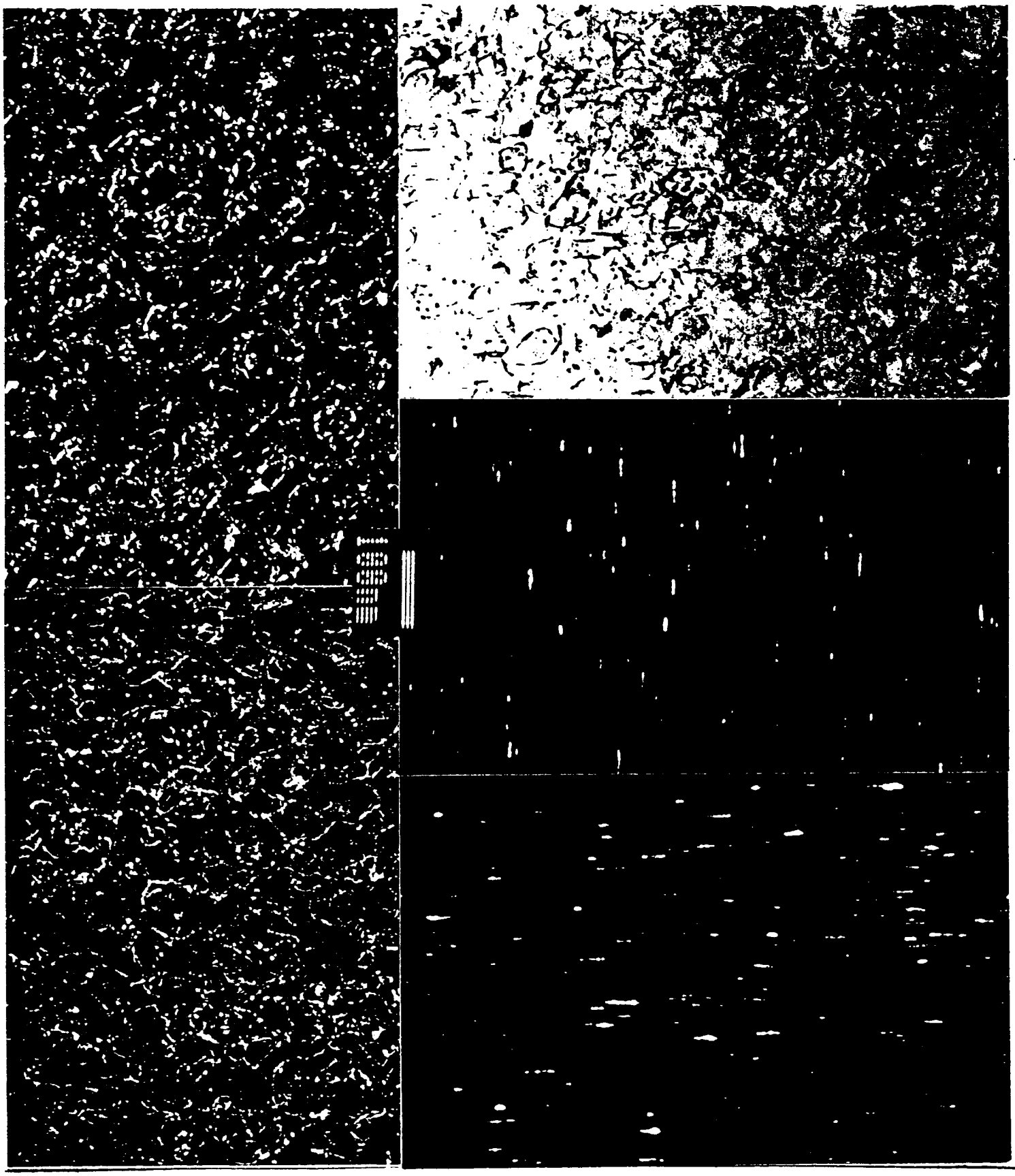

Fig 4

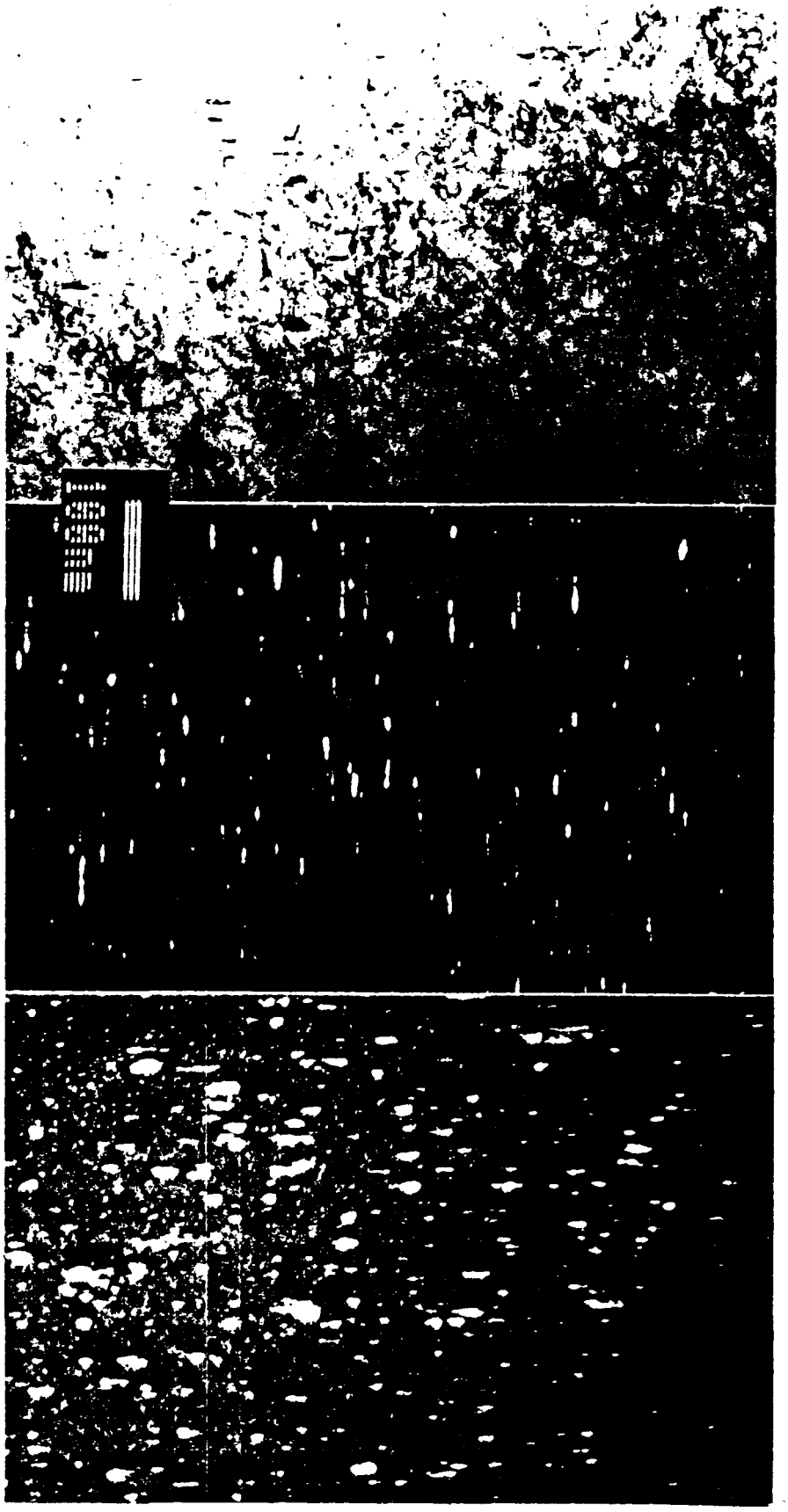

Fig. 5

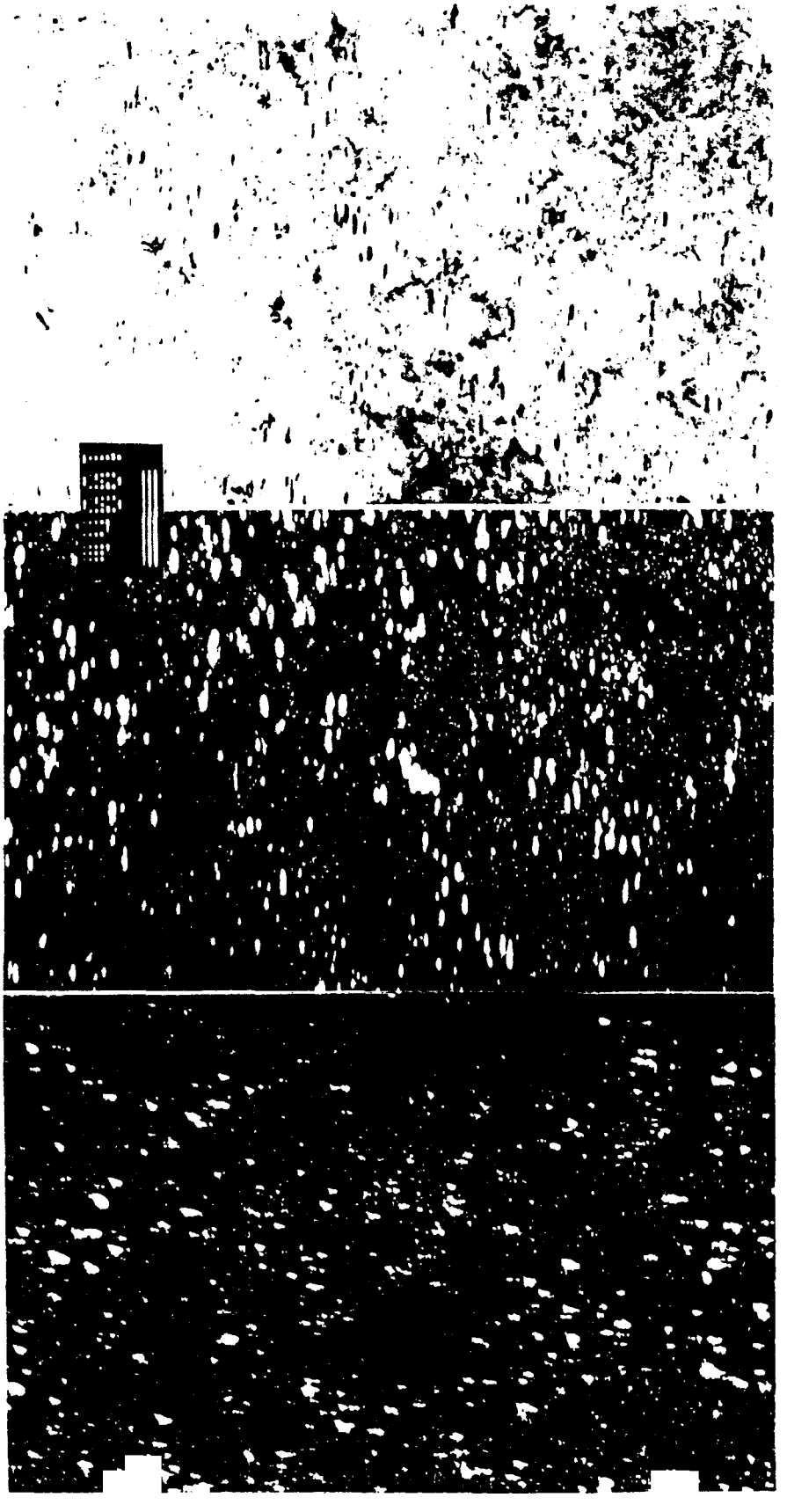

100nm

Fig. 7

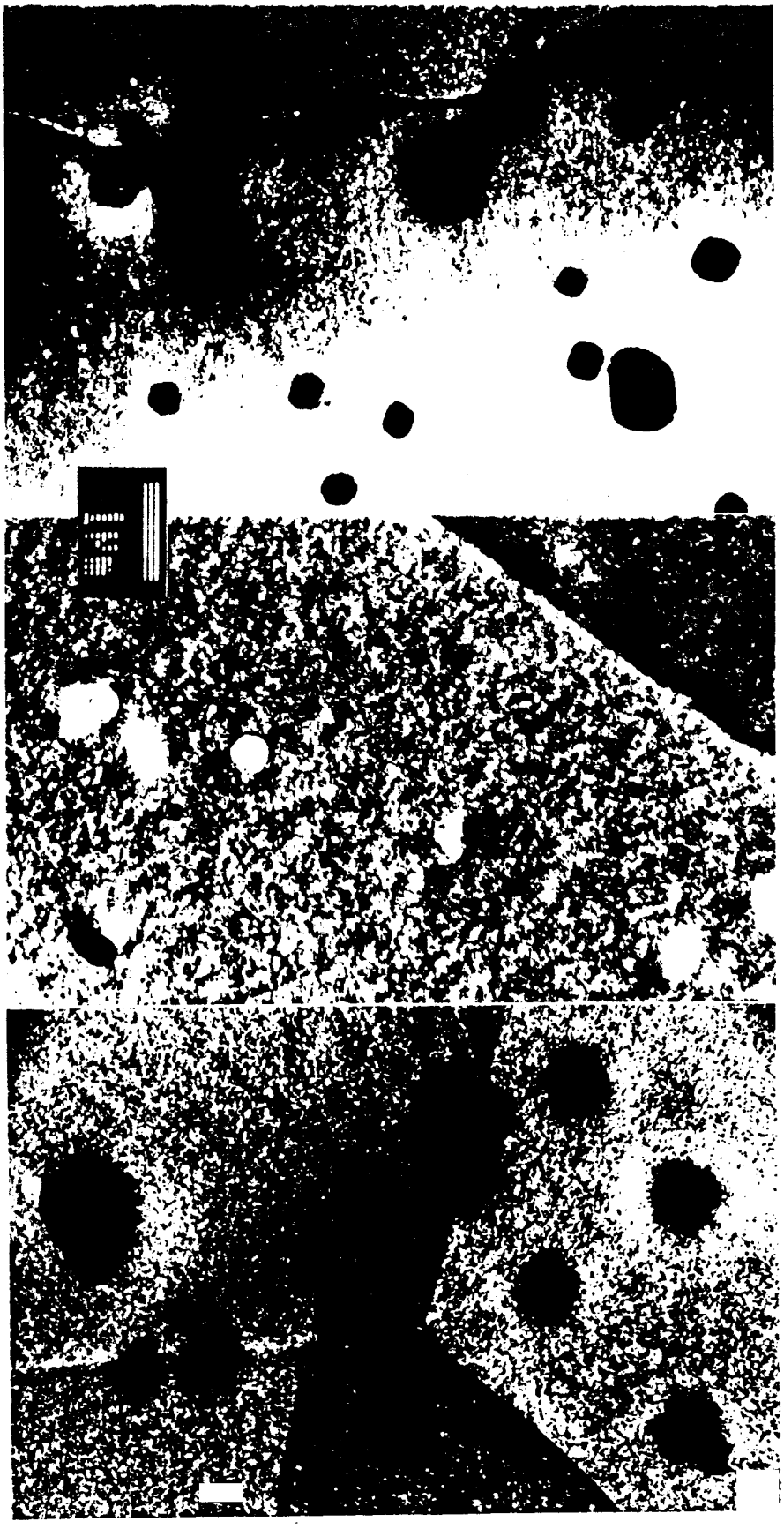

Fig. 8

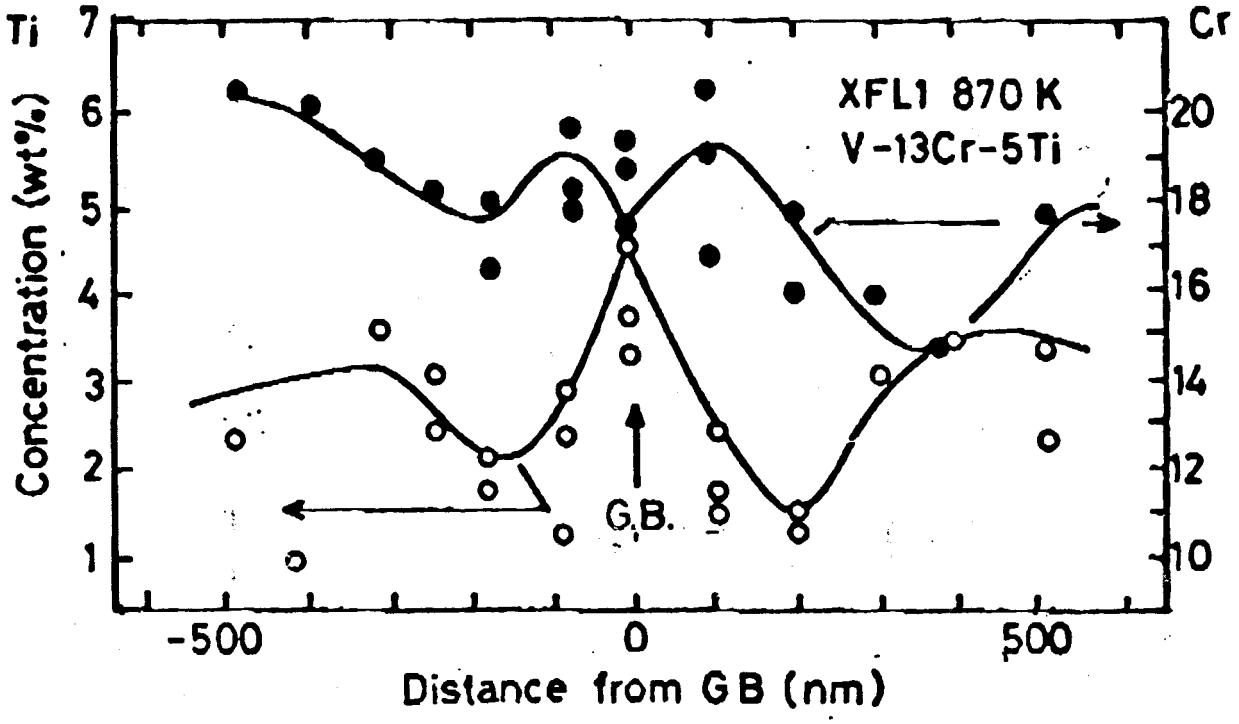
Ti
Cr
Concentration (wt%)
XFL1 870 K
V-13Cr-5Ti
G.B.
-500
0
500
Distance from GB (nm)